Vesicle shape, molecular tilt, and the suppression of necks

Hongyuan Jiang,[1] Greg Huber,[2] Robert A. Pelcovits,[3] and Thomas R. Powers[1]

[1]*Division of Engineering, Box D, Brown University, Providence, Rhode Island 02912, USA*

[2]*Center for Cell Analysis & Modeling, and Department of Cell Biology, University of Connecticut Health Center, Farmington, Connecticut 06030, USA*

and Department of Mathematics, University of Connecticut, Storrs, Connecticut 06269, USA

[3]*Department of Physics, Brown University, Providence, Rhode Island 02912, USA*

Can the presence of molecular-tilt order significantly affect the shapes of lipid bilayer membranes, particularly membrane shapes with narrow necks? Motivated by the propensity for tilt order and the common occurrence of narrow necks in the intermediate stages of biological processes such as endocytosis and vesicle trafficking, we examine how tilt order inhibits the formation of necks in the equilibrium shapes of vesicles. For vesicles with a spherical topology, point defects in the molecular order with a total strength of +2 are required. We study axisymmetric shapes and suppose that there is a unit-strength defect at each pole of the vesicle. The model is further simplified by the assumption of tilt isotropy: invariance of the energy with respect to rotations of the molecules about the local membrane normal. This isotropy condition leads to a minimal coupling of tilt order and curvature, giving a high energetic cost to regions with Gaussian curvature and tilt order. Minimizing the elastic free energy with constraints of fixed area and fixed enclosed volume determines the allowed shapes. Using numerical calculations, we find several branches of solutions and identify them with the branches previously known for fluid membranes. We find that tilt order changes the relative energy of the branches, suppressing thin necks by making them costly, leading to elongated prolate vesicles as a generic family of tilt-ordered membrane shapes.

I. INTRODUCTION

The interplay of surface curvature and liquid-crystalline order finds its fullest expression in the manifold and complex biological realizations of the bilayer membranes surrounding cells and intracellular organelles. Helfrich [1] connected membrane shape and molecular order, by realizing that the spontaneous curvature of a bilayer membrane could arise from the spontaneous splay of the ordered rodlike lipid molecules comprising the membrane. But the biological world offers richer varieties of orientational order and shape that remain to be understood. For example, lipid molecules typically tilt relative to the normal of the membrane [2–4], and it has recently become possible to image tilt-ordered domains on the surface of curved, micron-scale membranes [5]. Furthermore, curvature has proven to play an active role in cellular and subcellular processes [6]. Narrow necks with small mean curvature but large negative Gaussian curvature are relevant to biological membranes that compartmentalize through budding, since this neck geometry allows separate membrane-bound compartments to be budded off, while avoiding high-energy membrane shapes. Neck formation is universal and crucial to the phenomena of endo- and exocytosis [7,8], viral entry and budding, the traffic of continual fusion and fission of vesicle and Golgi membrane, and the interconnections between Golgi stacks [9] and between the smooth and rough endoplasmic reticulum. Because of the close association of these phenomena with cell function, it is crucial to understand the forces on membrane necks and the constraints on their formation.

In this paper we numerically calculate the equilibrium shapes of axisymmetric vesicles with tilt order. Figure 1 shows how dramatic the effect of tilt can be. The two vesicles have the same resistance to bending, the same enclosed volume, and the same area, but the one on the right has tilt order whereas the one on the left has no tilt order. As we review below, the tilt order may be described by a vector field which is tangent to the vesicle surface. Molecular interactions prefer uniform tilt order, which may be realized on a surface with zero Gaussian curvature such as a plane or the surface of a cylinder. But it is impossible to have a uniform vector field on a surface with nonzero Gaussian curvature, such as a sphere or the neck connecting the two spheres. Therefore, uniform molecular order and Gaussian curvature are incompatible [10,11]. In particular, as long as the molecular interactions are strong enough, the elongated prolate shape of Fig. 1 will be preferred over a shape with a neck.

We begin with a brief discussion of the relation of our work to previous work on membrane shapes and orientational order. Section III describes our minimal isotropic tilt model, coordinates, and numerical method. Our analysis and methods are straightforward, but we describe them here to make our paper self-contained. In Sec. IV we present the main results, which are the energy as a function of reduced volume for several different branches of solutions, and phase diagrams for shapes. In the final section we discuss the implications and limitations of our analysis.

II. RELATION TO PREVIOUS WORK

The equilibrium shapes of closed fluid membrane vesicles have been studied theoretically and experimentally for many years (see [12,13], and references therein). In the spontaneous-curvature model described by Helfrich, a patch
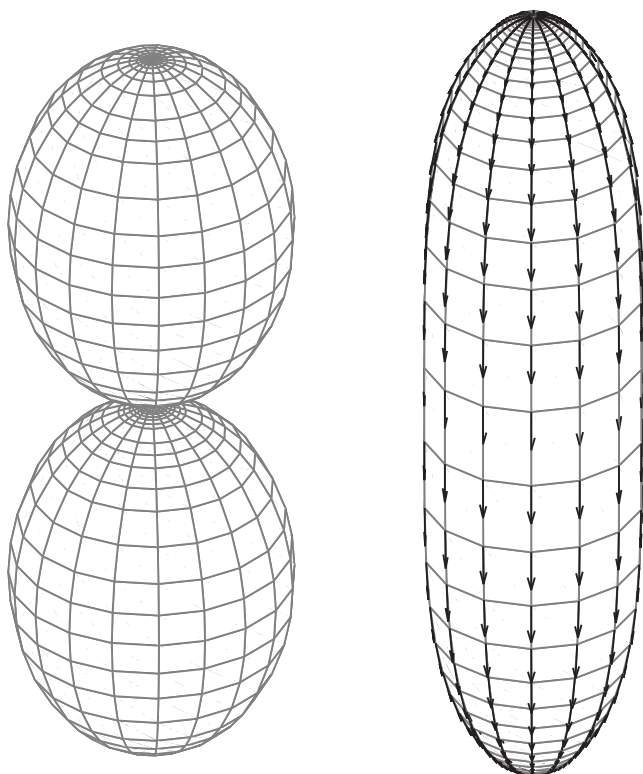
FIG. 1. Effect of tilt order on membrane shape. Left: fluid membrane with reduced volume $v=0.706$ and spontaneous curvature $c_0=2.4/R_0$, where R_0 is an overall length scale defined in Sec. III. Right: Tilt-ordered membrane with same parameters and tilt modulus $K_m=2.0\kappa$, where κ is the bending stiffness of the membrane. The arrows represent the tilt order. A +1 defect sits at both the north and the south poles of the vesicle.

of membrane has a resistance to bending but is curved in the absence of external loads [1]. A different approach known as the bilayer-coupling model accounts for the bilayer structure of a membrane by imposing a constraint on the number of molecules in both monolayers [14,15]. Both models predict the same set of vesicle shapes. However, the spontaneous-curvature model predicts that most shape transitions are discontinuous, while the bilayer-coupling model predicts continuous transitions [16]. To simplify our discussion, we will consider the spontaneous-curvature model with tilt order.

As alluded to above, the basic physics governing the interaction of vesicle shape and orientational order is the incompatibility of Gaussian curvature and uniform order. This incompatibility is a local property: a patch of surface with Gaussian curvature cannot have uniform tilt order. The global topology of surfaces also constrains the number and strength of point defects in the orientation order field, via the Poincáre-Brouwer theorem, which states that the total defect strength of a vector field on a surface is equal to the Euler characteristic (see [17] for an elementary proof). In our problem, a point defect is an isolated point where the tilt order vanishes, and the strength of the defect is the number of rotations of the tilt order field around that point. For a vesicle with the topology of a sphere, the total defect strength is +2. It is natural to suppose that the lowest energy states have two

+1 defects at antipodal points (we shall impose this two-defect configuration).

MacKintosh and Lubensky modeled a vesicle with spherical topology made up of molecules undergoing a transition from an untilted smectic-*A* phase to a tilted smectic-*C* phase [10]. They found that an initially spherical vesicle elongates into a prolate shape, with most of the Gaussian curvature concentrated near the defects that form at the two poles. They calculated the change in shape for this transition assuming fixed area, but they did not constrain the enclosed volume. Other work has examined the transitions among spherical, cylindrical, and toroidal vesicles with orientational order, again without the constraint of fixed enclosed volume [11,18]. In the current work, we impose the more realistic double constraint of fixed volume and fixed area, and solve for the shape. Also, our numerical method allows us to study shapes with large deflections from the spherical geometry. Therefore we can study the effect of tilt order on nonspherical shapes such as the pears and oblates predicted by the fluid membrane model. Rather than studying the transition in the tilt order (as in [10]), we focus on the shape effect: the effect of the tilt modulus K_m (the elastic constant governing the resistance to nonuniform tilt order) on the overall membrane shape.

Topological defects can also form for geometrical reasons, even on surfaces such as tori which do not require any defects in orientational order. Our work is complementary to recent work on the formation and interaction of such defects on a fixed but arbitrarily curved surface [19,20]. Instead of prescribing the shape and solving for the orientational order field, we prescribe the positions of two defects and solve for the vesicle shape and tilt field. We disallow additional defect formation, and discuss the validity and limitations of this restriction in Sec. V.

III. THE MODEL AND ITS ANALYSIS

We make several simplifying assumptions in our analysis. Since the vesicles we consider are much larger than their constituent molecules, we use continuum mechanics in the long-wavelength approximation. Thermal fluctuations are disregarded. We assume that the vesicle shapes are surfaces of revolution, and the tilt configuration is axisymmetric. In particular, the defects required by topology are assumed to sit at the two poles of the vesicle. These assumptions reduce the partial differential equations governing the shape and tilt configuration to ordinary differential equations, which greatly simplifies our calculations. Also, we suppose that the bilayer membrane is thin compared to the characteristic size of the vesicle. Since the lipid bilayers are approximately two nanometers thick [4], this assumption is highly accurate for vesicles of micron size and larger. A consequence of this assumption is that stretching is much more costly than bending; therefore, we demand that the total area remain constant. And, although membranes are permeable to water, osmotic effects resist changes in volume [12], leading us to fix the volume. As we explain below, we use a minimal model for the orientational order, disregarding anisotropic couplings between the tilt field and the membrane curvature. We also
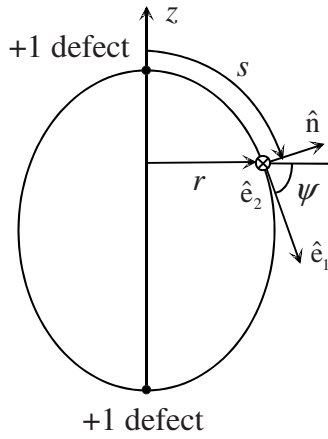
FIG. 2. Vesicle coordinate system and assumed location of defects. The shape is a surface of revolution about the z axis. The vector $\hat{\mathbf{e}}_2$ points into the page as indicated by the $\otimes$.

disregard chiral interactions, which have been shown to be important in models for lipid tubule structure [21,22] and a proposed mechanism for budding [23,24].

We will study how vesicle shape depends on area and volume in the presence of tilt order. Just as in the case of fluid membranes, we will see that the bending energy and tilt stiffness energy terms are scale invariant. This invariance allows us to vary area A and volume V by changing one parameter, the reduced volume v [12]. The reduced volume is the ratio of the actual volume of a vesicle to the volume of a sphere with the same area as the vesicle. If R_0 is the radius of the sphere with area A, then $v = V/(4\pi R_0^3/3)$.

A. Parametrization and geometry

In this section we describe our parametrization and fix the notation; see [25,17] for general discussions of differential geometry applied to membranes. We choose the z axis to be the axis of symmetry of the vesicle and represent points on the surface of the vesicle by the three-dimensional vector $\mathbf{X}(\phi,s) = (r(s)\cos\phi, r(s)\sin\phi, z(s))$, where ϕ and r are plane polar coordinates in the xy plane, and s is the arclength measured from the north pole of the surface along a line of longitude (see Fig. 2). We define $\psi(s)$ to be the angle between the tangent vector $\partial_s\mathbf{X}$ along a longitude and the horizontal axis. Then $dz/dr = z_s/r_s = -\tan\psi(s)$, where $0 < \psi(s) < \pi$. In terms of ψ, we have $r_s = \cos\psi$ and $z_s = -\sin\psi$.

An orthonormal basis in the tangent plane of the surface is given by

$$\hat{\mathbf{e}}_1 = \partial_s\mathbf{X} = (\cos\psi\cos\phi, \cos\psi\sin\phi, -\sin\psi)$$

$$\hat{\mathbf{e}}_2 = \partial_\phi\mathbf{X}/|\partial_\phi\mathbf{X}| = (-\sin\phi, \cos\phi, 0), \qquad (1)$$

where the s and ϕ subscripts denote partial differentiation with respect to the coordinates s and ϕ, respectively. We construct the outward normal $\hat{\mathbf{n}}$ to the surface using the orthonormal frame:

$$\hat{\mathbf{n}} = \hat{\mathbf{e}}_1 \times \hat{\mathbf{e}}_2 = (\sin\psi\cos\phi, \sin\psi\sin\phi, \cos\psi). \qquad (2)$$

The metric tensor g_{ij} of the surface is given by

$$g_{ij} = \partial_i\mathbf{X} \cdot \partial_j\mathbf{X} = \begin{pmatrix} 1 & 0 \\ 0 & r^2 \end{pmatrix}, \qquad (3)$$

where the indices $i, j = 1, 2$ label the coordinates s and ϕ, respectively. As usual, we denote the inverse of the metric tensor by g^{ij}, and we use g^{ij} to raise indices. The second fundamental form K_{ij} is defined by

$$K_{ij} \equiv \hat{\mathbf{n}} \cdot \partial_i\partial_j\mathbf{X} = -\begin{pmatrix} \psi_s & 0 \\ 0 & r\sin\psi \end{pmatrix}. \qquad (4)$$

From the second fundamental form we construct the mean curvature H and Gaussian curvature K:

$$H \equiv -\frac{1}{2}g^{ij}K_{ij} = \frac{1}{2}(\psi_s + \sin\psi/r) \qquad (5)$$

$$K \equiv \det(K^i{}_j) = \det(g^{il}K_{lj}) = \psi_s\sin\psi/r, \qquad (6)$$

where repeated indices have been summed over. Note from Eq. (5) that we use a convention in which the sphere has positive mean curvature.

We assume that the lipid molecules on the surface of the vesicle are tilted at a preferred angle with respect to the surface normal $\hat{\mathbf{n}}$, as in a smectic-C phase [32]. Let the vector $\mathbf{m}$ denote the projection of the directors of the lipid molecules onto the tangent plane. Since we do not study the transition between tilted and untilted phases, it is convenient to normalize $\mathbf{m}$ to make $|\mathbf{m}| = 1$ well away from topological defects. In terms of the local orthonormal basis of the tangent plane, we have

$$\mathbf{m} = B(\cos\theta\hat{\mathbf{e}}_1 + \sin\theta\hat{\mathbf{e}}_2) = B\hat{\mathbf{m}}, \qquad (7)$$

where the amplitude B vanishes at defect centers, and approaches unity far from defect cores.

We must assign an energy penalty to nonuniform configurations of the tilt field $\mathbf{m}$. For a flat surface, $\mathbf{m}$ is uniform if the components of $\mathbf{m}$ are constant in the standard Cartesian basis. Thus, a suitable energy density would be proportional to $\partial_i m^j \partial_i m^j$. However, on a curved surface, $\mathbf{m}$ can vary with position not only because m^i varies with position, but also because $\hat{\mathbf{e}}_i$ can vary. Furthermore, it is only the tangential component of derivatives of $\mathbf{m}$ that enter the tilt stiffness terms; normal components add to the resistance to bending and therefore may be absorbed in the bending energy term, discussed below. These features are captured by the covariant derivative

$$D_i\mathbf{m} = \partial_i\mathbf{m} - (\hat{\mathbf{n}}\cdot\partial_i\mathbf{m})\hat{\mathbf{n}} = (\partial_i m^1 - m^2\Omega_i)\hat{\mathbf{e}}_1 + (\partial_i m^2 + m^1\Omega_i)\hat{\mathbf{e}}_2, \qquad (8)$$

where the "spin connection,"

$$\Omega_i = \hat{\mathbf{e}}_2 \cdot \partial_i\hat{\mathbf{e}}_1, \qquad (9)$$

is the rate at which the frame $\{\hat{\mathbf{e}}_1, \hat{\mathbf{e}}_2\}$ rotates about the normal $\hat{\mathbf{n}}$ as the ith coordinate increases. The covariant curl of the spin connection is the Gaussian curvature:

$$K = -\frac{1}{\sqrt{g}}\epsilon_{ij}\partial_i\Omega_j, \tag{10}$$

where g is the determinant of the metric tensor and ϵ_{ij} is the antisymmetric symbol with $\epsilon_{12}=1$ [17]. We can now see why Gaussian curvature is incompatible with a uniform tilt field. Consider a tilt field on a surface of nonzero Gaussian curvature. A tilt field on a curved surface is uniform if it has a vanishing covariant derivative. Writing Eq. (8) in terms of B and θ, we find that $D_i\mathbf{m}=0$ implies $\partial_i B=0$ and $\partial_i\theta+\Omega_i=0$. Consider a patch on a curved surface that includes no defects, so that θ is smooth. Then, to solve $\partial_i\theta+\Omega_i=0$ for θ we must have $\epsilon_{ij}\partial_i\Omega_j=0$ [17]. Therefore, the tilt field cannot be uniform on a patch with Gaussian curvature.

For our parametrization, $\Omega_i=(0,\cos\psi)$: the frame $\{\hat{\mathbf{e}}_1,\hat{\mathbf{e}}_2\}$ rotates about the normal as ϕ changes, but not as s changes. Consistent with our assumption that the shape of the surface is axisymmetric, we assume that the orientation of the molecules is axisymmetric as well, with $\partial_\phi B=0$ and $\partial_\phi\theta=0$. Therefore,

$$D_\phi\mathbf{m} = B\cos\psi\,\hat{\mathbf{m}}_\perp \tag{11}$$

$$D_s\mathbf{m} = B_s\hat{\mathbf{m}} + B\theta_s\hat{\mathbf{m}}_\perp, \tag{12}$$

where $\hat{\mathbf{m}}_\perp=-\sin\theta\hat{\mathbf{e}}_1+\cos\theta\hat{\mathbf{e}}_2$, $B_s=\partial_s B$, and $\theta_s=\partial_s\theta$.

B. Free energy

The free energy F of the vesicle is the sum of terms associated with the bending of the vesicle and terms associated with the tilt vector order parameter field: $F=F_b+F_m$. We use the Helfrich model for bending energy,

$$F_b = \int\left[\frac{\kappa}{2}(2H-c_0)^2 + \kappa_G K\right]\sqrt{g}\,ds\,d\phi. \tag{13}$$

In Eq. (13), κ is the bending modulus, typically $10-15k_BT$ [4], and κ_G is the Gaussian rigidity. The spontaneous curvature c_0 is twice the preferred value of the mean curvature for a patch of membrane. Spontaneous curvature of a bilayer membrane can arise either from the sum of the inherent spontaneous curvatures of the monolayers, or from a difference in the number of molecules in either monolayer [26]. Since we consider a closed surface with fixed topology, the Gauss-Bonnet theorem ensures that the integral of the Gaussian curvature is independent of shape and contributes only an overall constant to the free energy [33]. Therefore the term proportional to κ_G may safely be disregarded.

The elastic free energy F_m for the tilt order is a sum of many terms, including costs for splay and bend of the director field, and many terms coupling the director field to the vesicle shape [27,28]. To simplify our task, we demand that the energy be isotropic in tilt, i.e., invariant under arbitrary rotations of $\mathbf{m}$ about the normal $\hat{\mathbf{n}}$. This symmetry rules out all of the anisotropic terms, leaving only a minimal coupling of the tilt order to shape:

$$F_m = \frac{1}{2}\int\left[K_m D_i m^j D^i m_j + \frac{\lambda}{2}(1-m_i m^i)^2\right]\sqrt{g}\,ds\,d\phi. \tag{14}$$

The first term of Eq. (14) gives a preference for a uniform tilt field. Since we impose isotropy, the free energy density at a point is independent of the direction of $\mathbf{m}$ relative to the principal directions of curvature. (We discuss how anisotropy may affect our results in Sec V.) Note that the Frank elastic constant K_m has the same dimensions as κ, implying that the effects of this term are comparable to the effects of the bending term of Eq. (13). We know of no measurements of K_m in vesicles, but by dimensional analysis we expect that K_m is comparable to κ. This argument gives good estimates for the Frank constants in three-dimensional liquid crystal systems [32]. In the absence of concrete measurements, our calculations will explore a reasonable range of K_m/κ. The second term of Eq. (14) gives a preference for $|\mathbf{m}|=1$. We assume that we are deep in the ordered phase, so that $\lambda R_0^2/K_m\gg 1$. The length scale $\sqrt{K_m/\lambda}$ determines the radius of the defect core, wherein $|\mathbf{m}|$ falls steeply to zero.

The shape of the vesicle and the orientation of the tilted molecules on its surface are determined by minimizing F subject to a given surface area A and volume V. To impose these constraints, we introduce Lagrange multipliers Σ and P. It is convenient to treat r and ψ as independent variables in the variation of the free energy. Therefore, we introduce an additional Lagrange multiplier function $\gamma(s)$ to impose the local constraint $r_s=\cos\psi$. Thus, our task is to minimize

$$F' \equiv F + \Sigma A + PV + \kappa\int\gamma(s)(r_s-\cos\psi)\,ds\,d\phi. \tag{15}$$

It is convenient to scale the Lagrange multipliers by κ: $\bar{\Sigma}=\Sigma/\kappa$ and $\bar{P}=P/\kappa$. Then F' can be written as

$$F' = 2\pi\kappa\int_0^L f'(\psi,\psi_s,r,r_s,B,B_s,\theta_s,\gamma)\,ds, \tag{16}$$

where the upper integration limit L is the total arclength along a longitude from the north to the south pole, and

$$\begin{aligned}f'(\psi,\psi_s,r,r_s,B,B_s,\theta_s,\gamma) = r\Bigg[&\frac{1}{2}(\sin\psi/r+\psi_s-c_0)^2 + \bar{\Sigma}\\ &+\frac{1}{2}\bar{P}r\sin\psi + \frac{\lambda}{4\kappa}(1-B^2)^2\\ &+\frac{K_m}{2\kappa}(B^2\cos^2\psi/r^2+B_s^2+B^2\theta_s^2)\Bigg]\\ &+\gamma(s)(r_s-\cos\psi).\end{aligned} \tag{17}$$

C. Euler-Lagrange equations

The Euler-Lagrange equations which extremize F' are given by

$$\psi_s = \frac{U}{r} - \frac{\sin\psi}{r} + c_0, \tag{18}$$

$$U_s = \frac{U}{r} \cos \psi + \gamma \sin \psi + \frac{1}{2} \bar{P} r^2 \cos \psi - \frac{K_m B^2}{\kappa r} \cos \psi \sin \psi, \tag{19}$$

$$B_s = \frac{\kappa W}{K_m r}, \tag{20}$$

$$W_s = -\frac{\lambda}{\kappa} r B (1 - B^2) + \frac{K_m r B}{\kappa} \left(\frac{\cos^2 \psi}{r^2} + \theta_s^2 \right), \tag{21}$$

$$\gamma_s = \frac{U^2}{2r^2} - \frac{U}{r^2} \sin \psi + \bar{P} r \sin \psi + \bar{\Sigma} + \frac{K_m}{2\kappa} \left[-\frac{B^2}{r^2} \cos^2 \psi \right.$$
$$\left. + \left(\frac{\kappa W}{K_m r} + B^2 \theta_s^2 \right)^2 \right] + \frac{\lambda}{4\kappa} (1 - B^2)^2, \tag{22}$$

$$r_s = \cos \psi, \tag{23}$$

$$(r B^2 \theta_s)_s = 0. \tag{24}$$

We have introduced two auxiliary functions U and W to obtain first-order differential equations, which are required for our numerical routine.

The Euler-Lagrange equations can be simplified somewhat by the observation that θ is independent of s. Equation (24) implies that $r B^2 \theta_s$ is independent of s. However, because r and B both vanish at the poles, $r K_m' B^2 \theta_s = 0$ everywhere. Since B and r are nonzero only right at the poles, $\theta_s = 0$ everywhere. This result can be seen more directly by examining the form of the free energy F_m, Eq. (14). Since $\Omega_s = \Omega_1 = 0$, F_m is minimized when θ is independent of s. Note that the isotropy of the energy means that F is independent of the angle θ. In Fig. 1, for example, we chose to have the directors aligned with lines of latitude. The choice was arbitrary—directors aligned along lines of longitude, or any other direction, would result in the same free energy and same shape.

For the remaining six equations (18)–(23), we have six corresponding boundary conditions. The angle ψ and radius r are fixed at either pole: $\psi(0) = r(0) = r(L) = 0$, and $\psi(L) = \pi$. The amplitude B at either pole vanishes due to the assumed presence of defects, $B(0) = B(L) = 0$. However, L is still unknown and must be solved for along with the shape. To determine L, we reparametrize the problem, introducing a new independent variable t such that $t = 0$ at the north pole and $t = 1$ at the south pole: $s = Lt$, where L is a constant [29]. The Euler-Lagrange equations (18)–(24) are therefore modified by replacing d/ds with $(1/L)d/dt$. Note that the boundary conditions on r, ψ, and B at $s = L$ become boundary conditions at $t = 1$. The additional equation allowing us to solve for L is $dL/dt = 0$. To determine the additional boundary condition required by this equation, we consider the symmetry of the free energy under a constant shift in s. The free energy density now takes the form $F' = 2\pi\kappa \int_0^1 \tilde{f} dt$, where

$$\tilde{f}(\psi, \psi_t, r, r_t, B, B_t, \theta_t, \gamma, s_t) = s_t f'(\psi, \psi_s/L, r, r_s/s_t, B, B_s/s_t, \theta_s/s_t, \gamma), \tag{25}$$

and $s_t = L$. Since $s(t)$ does not appear explicitly in the free energy density, there is a first integral or Hamiltonian function $\partial \tilde{f}/\partial s_t$ which is independent of t. Examination of the variation of $\tilde{f}$ with respect to $s(t)$ leads to $\partial \tilde{f}/\partial s_t = 0$ at $t = 1$, implying that the Hamiltonian function vanishes everywhere. Writing the Hamiltonian explicitly in terms of the dependent variables at $t = 0$ yields the desired boundary condition $\gamma(0) = 0$ [16,29].

To complete our specification of the shape equations, we describe how we implement the constraints of fixed area and volume. It is convenient to regard area as a function of t. We define $A(t)$ as the area of the portion of the vesicle surface north of the line of latitude corresponding to t, with a similar definition for $V(t)$. Then

$$A_t = 2\pi r L \tag{26}$$

$$V_t = \pi r^2 \sin \psi L \tag{27}$$

$$\bar{\Sigma}_t = 0 \tag{28}$$

$$\bar{P}_t = 0, \tag{29}$$

where Eqs. (28) and (29) arise because the Lagrange multipliers are constant, but unknown and shape dependent. The four boundary conditions corresponding to Eqs. (26)–(29) are $A(0) = 0$, $A(1) = 4\pi R_0^2$, $V(0) = 0$, and $V(1) = 4\pi R_0^3 v/3$. The scale R_0 is set to unity in our numerical calculations. Finally, the shape is determined by integrating $z_t = -L \sin \psi$ with boundary condition $z(0) = 0$.

Although the Euler-Lagrange equations are nonlinear and must be solved numerically, it is straightforward to determine the form of the amplitude B at the centers of the defect cores. For example, near $s = 0$, we have $\cos \psi \approx 0$ and $r \approx s$. Therefore, Eqs. (20) and (21) reduce to Bessel's equation for $s \approx 0$:

$$s^2 B_{ss} + s B_s + \left(\frac{\lambda}{K_m} s^2 - 1 \right) B = 0, \tag{30}$$

and thus $B \propto s$ in the core, which has a size set by $\sqrt{K_m/\lambda}$, as mentioned earlier. Similar considerations apply to the defect located at the south pole.

In our numerical approach, we treat the Euler-Lagrange equations as a two-point boundary value problem, using the MATLAB function bvp4c [30]. We choose $\lambda/K_m = 1000$ to make the defect cores small. To avoid the divergences that occur in the equations when $r \to 0$, we solve the equations in the interval $\delta < t < 1 - \delta$, where $\delta = 0.001$. All boundary conditions are now evaluated at $t = \delta$ or $t = 1 - \delta$. We use Taylor series to relate the boundary values at these end points to the values at $t = 0$ and $t = 1$:

$$\psi(\delta) \approx \psi(0) + \psi_t(0)\delta = \psi_t(0)\delta \tag{31}$$

$$B(\delta) \approx B(0) + B_t(0)\delta = B_t(0)\delta \tag{32}$$

$$\psi(1 - \delta) \approx \psi(1) - \psi_t(1)\delta = \pi - \psi_t(1)\delta \qquad (33)$$

$$B(1 - \delta) \approx B(1) - B_t(1)\delta = -B_t(1)\delta. \qquad (34)$$

The constants $\psi_t(0)$, $B_t(0)$, $\psi_t(1)$, and $B_t(1)$ are unknown parameters that may be determined by the numerical routine using the conditions

$$U(\delta) \approx L\psi_t(\delta)r(\delta) + \sin(\psi(\delta)) + c_0 r(\delta) \qquad (35)$$

$$U(1 - \delta) \approx L\psi_t(1 - \delta)r(1 - \delta) + \sin(\psi(1 - \delta)) + c_0 r(1 - \delta) \qquad (36)$$

$$W(\delta) \approx LB_t(\delta)K_m r(\delta)/\kappa \qquad (37)$$

$$W(1 - \delta) \approx LB_t(1 - \delta)K_m r(1 - \delta)/\kappa. \qquad (38)$$

from Eqs. (18) and (20). We also have

$$\gamma(\delta) = \gamma(0) + \gamma_t(0)\delta \approx \gamma(0) + \gamma_t(\delta)\delta = \gamma_t(\delta)\delta, \qquad (39)$$

with an error of order δ^2. The parameter $\gamma_t(\delta)$ is given in terms of the variables at $t = \delta$ by Eq. (22).

IV. RESULTS

For purposes of comparison with the case of a fluid membrane with no tilt order, we have repeated the calculations of Ref. [16] for spontaneous curvature $c_0 = 0$ and $c_0 R_0 = 2.4$. At $v = 1$, the vesicle shape is always spherical, with bending energy $8\pi\kappa$. First consider the case $c_0 = 0$. As v is decreased from unity, the lowest energy shape becomes prolate, elongating continuously. Upon further decrease of v, the shape changes discontinuously to oblate, and finally to the stomatocyte shape. At $v = 0$ where the dashed-dotted line in Fig. 3(a) terminates, the stomatocyte shape consists of two concentric spheres, spaced infinitesimally close, connected by a vanishingly thin neck of zero mean curvature, with a total bending energy $16\pi\kappa$. Figure 3(a) shows some of these shapes, and the free energy vs v over the range for which the transitions occur. Note that there are two stomatocyte branches; the upper one (dotted line) is metastable. As the reduced volume is decreased along the upper stomatocyte branch, the vesicle height along the z axis decreases and the shape becomes more symmetric about the horizontal plane midway between the two defects. The two branches join at the filled circle, where the stomatocyte shape becomes oblate. Figures 3(b) and 3(c) show the effect of tilt order. As K_m/κ increases, the prolate branch of solutions has lower free energy than the oblate branch for a greater range of reduced volume, until eventually the oblate branch becomes completely metastable. To understand why tilt order favors prolate shapes over oblate, note that as v decreases, the prolate shapes extend more along the z axis and become more cylindrical, leading to a greater region of small Gaussian curvature and approximately uniform tilt order. The oblate shapes also have regions of small Gaussian curvature, but these regions are confined to narrow bands near $t \approx 0.2$ and $t \approx 0.8$ (Fig. 4).

Figure 4 also shows that our assumption that the defects are constrained to lie at the poles of the vesicle is reasonable.
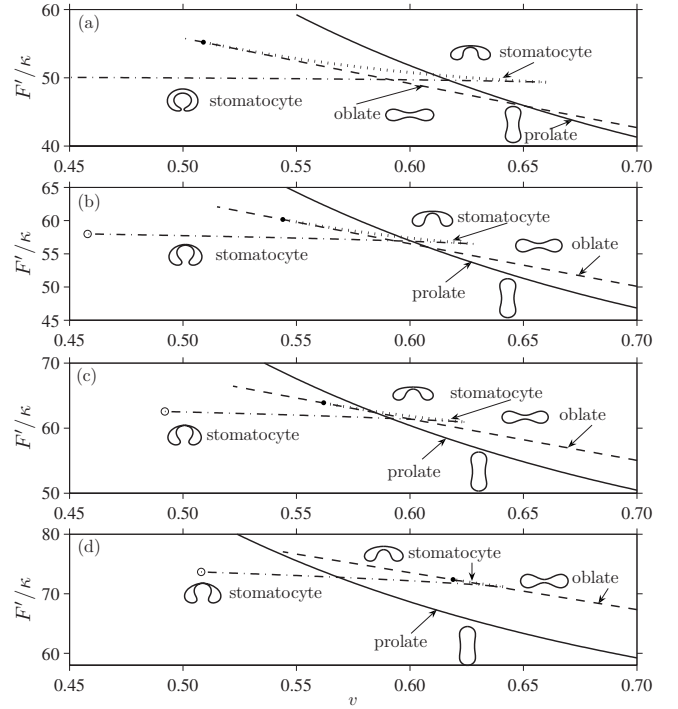

FIG. 3. Dimensionless free energy F'/κ vs reduced volume v for fluid membrane vesicles with $c_0 = 0$ for three different values of Frank elastic constant: (a) $K_m = 0$. (b) $K_m = 0.3\kappa$. (c) $K_m = 0.5\kappa$. (d) $K_m = \kappa$. Solid lines correspond to prolate shapes, dashed lines correspond to oblate shapes, and the dashed-dotted and dotted lines correspond to stomatocyte shapes. The filled circles denote continuous bifurcations. The open circles denote limit points at which the vesicle intersects itself.

Defects of positive sign prefer regions of positive Gaussian curvature [31]. Figure 4 shows that for $K_m/\kappa \lesssim 0.5$, the Gaussian curvature at the equator is just greater than the Gaussian curvature at either pole. Thus, for $K_m \lesssim 0.5\kappa$, we expect that the configuration with two defects at antipodal points on the equator might have smaller energy than the configuration with defects on either pole. Our simplifying assumption of axisymmetry prevents us from investigating this possibility. However, as K_m/κ is increased to unity, the regions of maximum Gaussian curvature lie at the poles, and we expect that the minimum energy configuration is to have
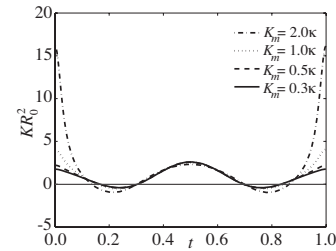

FIG. 4. Dimensionless Gaussian curvature KR_0^2 vs the dimensionless parameter t for oblate shapes with $c_0 = 0$ and various values of K_m/κ. Note that $t = 0$ at the north pole, $t = 1$ at the south pole, and $t = 0.5$ at the equator, which lies in the horizontal plane midway between the two defects.
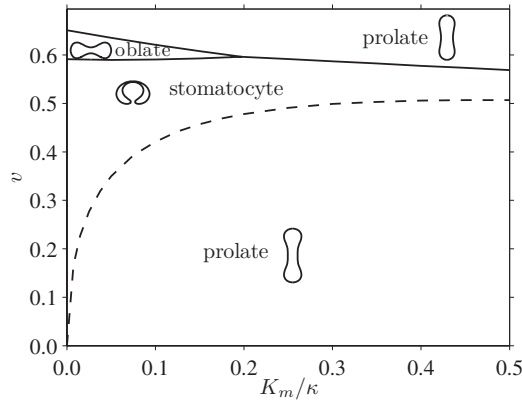
FIG. 5. Phase diagram for lowest energy vesicle shapes for c_0 = 0. The lowest energy shapes are shown for each value of v and K_m/κ. The dashed line denotes the line of limit points for the stomatocyte shapes.

the defects lie at the poles. For the prolate shapes and the pear shapes considered below, the poles are always regions of maximum Gaussian curvature. Even for the stomatocyte, the north pole is the region of maximum Gaussian curvature, and the Gaussian curvature is roughly constant over much of the inner surface of the pocket.

A second qualitative effect of tilt order on the c_0 = 0 shapes is that the lower stomatocyte branch develops a limit point corresponding to self-intersection at the sites of the defects. These limit points are denoted by open circles in Figs. 3(b) and 3(c). Figure 5 shows the phase diagram for the lowest energy vesicle shapes for the case c_0 = 0 as a function of the Frank constant. The dashed line shows the values of K_m/κ and v for which the stomatocyte shape intersects itself. For values of v below the dashed line, the prolate branch again becomes the lowest energy branch of solutions.

Turning to the case $c_0 R_0$ = 2.4, we see from Ref. [16] that the fluid membrane shapes are dominated by prolate shapes and pear shapes, Fig. 6(a). Note that the energy scale on the vertical axis is much less than that of Fig. 3(a) since the mean curvature required by the constraints of fixed volume and area is close to c_0. The solid dots again denote continuous transitions between pear and prolate shapes. The effect of tilt order is to increase the energy cost of the pear shapes relative to the prolate shapes, eventually making the prolate branch of solutions the lowest energy branch for all v. It is interesting to note that tilt order does not completely rule out pear shapes with narrow necks. The phase diagram of lowest energy shapes in Fig. 7 shows that pear shapes are allowed in a range of v for sufficiently small K_m. The neck of the pear shape becomes wider as K_m increases. For these shapes, there is a slight reduction in the order B in a narrow band around the neck.

V. DISCUSSION AND CONCLUSION

Our detailed, systematic calculations show that tilt order suppresses necks and favors elongated prolate shapes for sufficiently large tilt modulus K_m. We calculated the free energy
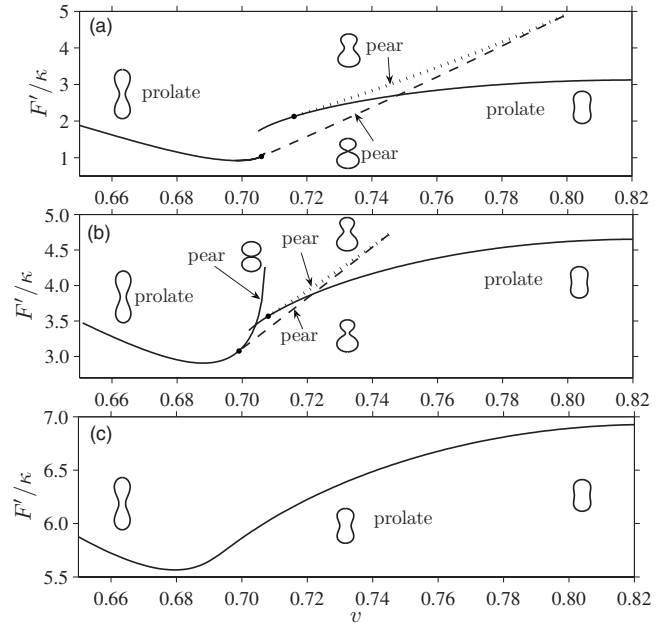

FIG. 6. Dimensionless free energy F'/κ vs reduced volume v for fluid membrane vesicles with $c_0 R_0$ = 2.4 and three different values of Frank elastic constant: (a) K_m/κ = 0, (b) K_m/κ = 0.08, (c) K_m/κ = 2.0. Solid lines correspond to prolate shapes, dashed lines correspond to asymmetric pear shapes, and the dotted line corresponds to symmetric pear shapes. The filled circles mark continuous bifurcations. There is a symmetric pear branch in (a), just to the right of the first bifurcation, but it is too short to be seen.

as a function of reduced volume for several branches of solutions, and showed how increasing the tilt modulus increases the energy of the nonprolate branches relative to the prolate branches, finally leading to a single family of prolate shapes.

Our calculation was based on several important assumptions. We ruled out many of the possible terms in the free energy by taking the free energy to be invariant under arbitrary rotations of $\hat{\mathbf{m}}$ about the normal $\hat{\mathbf{n}}$. A natural way to remove this assumption and study the effects of anisotropy without introducing an unmanageable number of terms would be to replace F_m with F_d, the one-Frank-constant ap-
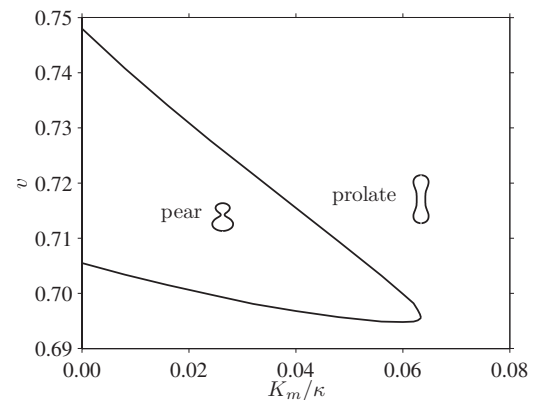

FIG. 7. Phase diagram for $c_0 R_0$ = 2.4. The lowest energy shapes are shown for each value of v and K_m/κ.

proximation for the orientational free energy of the directors $\hat{\mathbf{d}}$ making up the membrane surface [21]:

$$F_d = \frac{K_m}{2} \int (\partial_i \hat{\mathbf{d}} \cdot \partial_j \hat{\mathbf{d}}) g^{ij} \sqrt{g} \, ds \, d\phi. \tag{40}$$

To compare F_d with F_m, write $\hat{\mathbf{d}} = \alpha \hat{\mathbf{N}} + \mathbf{m}$, where $\hat{\mathbf{N}}$ is the local unit surface normal, and α is determined by $|\hat{\mathbf{d}}| = 1$. Rewriting F_d in terms of intrinsically two-dimensional quantities, we find that

$$F_d = \frac{K_m}{2} \int \big[g^{ij} \nabla_i m^k \nabla_j m_k + \alpha^2 K_i^j K_j^i + m^i K_{ij} K_k^j m^k$$
$$- 2\alpha (\nabla_i m^j) K_j^i \big] \sqrt{g} \, ds \, d\phi. \tag{41}$$

The first two terms of the integrand in Eq. (41) are isotropic. To see that the term $K_i^j K_j^i$ is already accounted for in our minimal isotropic tilt model, note that a matrix satisfies its own characteristic equation:

$$K_k^i K_j^k - K_j^i K_k^k + K \delta_j^i = 0. \tag{42}$$

Using g^{ij} to take the trace of Eq. (42) yields $K_j^i K_i^j = 4H^2 - 2K$. We expect that the term $m^i K_{ij} K_k^j m^k$ leads to a preference for the tilt to order along the long axis of a prolate shape, and an increased bending stiffness along the direction parallel to $\hat{\mathbf{m}}$. The last term in the integrand of Eq. (41) is like a spontaneous curvature given by a gradient of the projected director. Except for the fact that the anisotropic terms will lead to a preferred direction of $\hat{\mathbf{m}}$ relative to the principal directions of curvature, we expect that including these terms would not qualitatively change our results. A more dramatic change is expected if chiral terms like $m^i \epsilon_{ij} K_k^j m^k$ are allowed. This term can give the vesicle a chiral shape, which is necessarily non-axisymmetric. It would be interesting to add this term alone to our minimal model and study vesicles shapes, as has recently been done for tubules and ribbons [22].

The most severe assumption of our model is the assumption of fixed defects at the poles. We have already mentioned that positive sign defects prefer regions of positive curvature, which suggests there may be lower energy, non-axisymmetric shapes than the ones we consider here. Furthermore, recent calculations have shown how a pair of defects of opposite sign can be pulled apart whenever there is a change in sign in the Gaussian curvature, with the positive defect migrating to the region of positive Gaussian curvature, and the negative defect migrating to the region of negative Gaussian curvature [20]. The magnitude of the curvature in both regions is important for determining whether or not a defect pair will unbind. Although we completely disregard this effect, we expect it will not play much of a role in the low-energy prolate shapes, since for those shapes there are at most only narrow bands of mildly negative Gaussian curvature where either end starts to bow out. An important extension of our calculation would be to lift the assumption of axisymmetry, and allow both the defect position and number and vesicle shape to vary. It would be interesting if the techniques of Ref. [5] could be used to experimentally determine defect position on vesicles with tilt order.

Finally, we have systematically studied the effect of changing the tilt modulus K_m while deep in the ordered phase. While we have not presented results on the change in shape due to a phase transition from an ordered tilt phase to a disordered fluid phase, as in Ref. [10], we expect that the effect of increasing the order should be qualitatively similar to increasing K_m.

ACKNOWLEDGMENTS

[1] W. Helfrich, Z. Naturforsch. C **28c**, 693 (1973).

[2] G. S. Smith, E. B. Sirota, C. R. Safinya, and N. A. Clark, Phys. Rev. Lett. **60**, 813 (1988).

[3] G. S. Smith, E. B. Sirota, C. R. Safinya, R. J. Plano, and N. A. Clark, J. Chem. Phys. **92**, 4519 (1990).

[4] O. Mouritsen, *Life as a Matter of Fat: The Emerging Science of Lipidomics* (Springer-Verlag, Berlin, 2005).

[5] Y. Zhao, N. Mahajan, R. Lu, and J. Fang, Proc. Natl. Acad. Sci. U.S.A. **102**, 7438 (2005).

[6] H. T. McMahon and J. L. Gallop, Nature (London) **438**, 590 (2005).

[7] V. A. Frolov, V. A. Lizunov, A. Ya. Dunina-Barkovskaya, A. V. Samsonov, and J. Zimmerberg, Proc. Natl. Acad. Sci. U.S.A. **100**, 8698 (2003).

[8] T. Baumgart, S. T. Hess, and W. W. Webb, Nature (London) **425**, 821 (2003).

[9] J. Derganc, A. A. Mironov, and S. Svetina, Traffic (Oxford, U.

K.) **7**, 85 (2006).

[10] F. C. MacKintosh and T. C. Lubensky, Phys. Rev. Lett. **67**, 1169 (1991).

[11] T. C. Lubensky and J. Prost, J. Phys. II **2**, 371 (1992).

[12] U. Seifert, Adv. Phys. **46**, 13 (1997).

[13] H.-G. Döbereiner, E. Evans, M. Kraus, U. Seifert, and M. Wortis, Adv. Phys. **55**, 4458 (1997).

[14] S. Svetina and B. Zeks, Biomed. Biochim. Acta **42**, 86 (1983).

[15] S. Svetina and B. Zeks, Eur. Biophys. J. **17**, 101 (1989).

[16] U. Seifert, Karin Berndl, and Reinhard Lipowsky, Phys. Rev. A **44**, 1182 (1991).

[17] R. D. Kamien, Rev. Mod. Phys. **74**, 953 (2002).

[18] R. M. L. Evans, J. Phys. II **5**, 507 (1995).

[19] M. J. Bowick, D. R. Nelson, and A. Travesset, Phys. Rev. B **62**, 8738 (2000).

[20] V. Vitelli and D. R. Nelson, Phys. Rev. E **70**, 051105 (2004).

[21] J. V. Selinger, F. C. MacKintosh, and J. M. Schnur, Phys. Rev.

E **53**, 3804 (1996).

[22] Z. C. Tu and U. Seifert, e-print arXiv:cond-mat/0705.2707v1.

[23] R. C. Sarasij and M. Rao, Phys. Rev. Lett. **88**, 088101 (2002).

[24] R. C. Sarasij, S. Mayor, and M. Rao, Biophys. J. **92**, 3140 (2007).

[25] F. David, in *Statistical Mechanics of Membranes and Surfaces: Jerusalem Winter School for Theoretical Physics*, edited by D. R. Nelson, T. Piran, and S. Weinberg (World Scientific, Singapore, 1989).

[26] H.-G. Döbereiner, O. Selchow, and R. Lipowsky, Eur. Biophys. J. **28**, 174 (1999).

[27] P. Nelson and T. Powers, J. Phys. II **3**, 1535 (1993).

[28] T. Powers and P. Nelson, J. Phys. II **5**, 1671 (1995).

[29] F. Jülicher and R. Lipowsky, Phys. Rev. E **53**, 2670 (1996).

[30] L. F. Shampine, I. Gladwell, and S. Thompson, *Solving ODE's with MATLAB* (Cambridge University Press, New York, 2003).

[31] M. J. Bowick, D. R. Nelson, and A. Travesset, Phys. Rev. B **69**, 041102(R) (2004).

[32] P. G. de Gennes and J. Prost, *The Physics of Liquid Crystals*, 2nd ed. (Oxford University Press, Oxford, 1995).

[33] R. S. Millman and G. D. Parker, *Elements of Differential Geometry* (Prentice Hall, New York, 1977).